

1 Supporting information

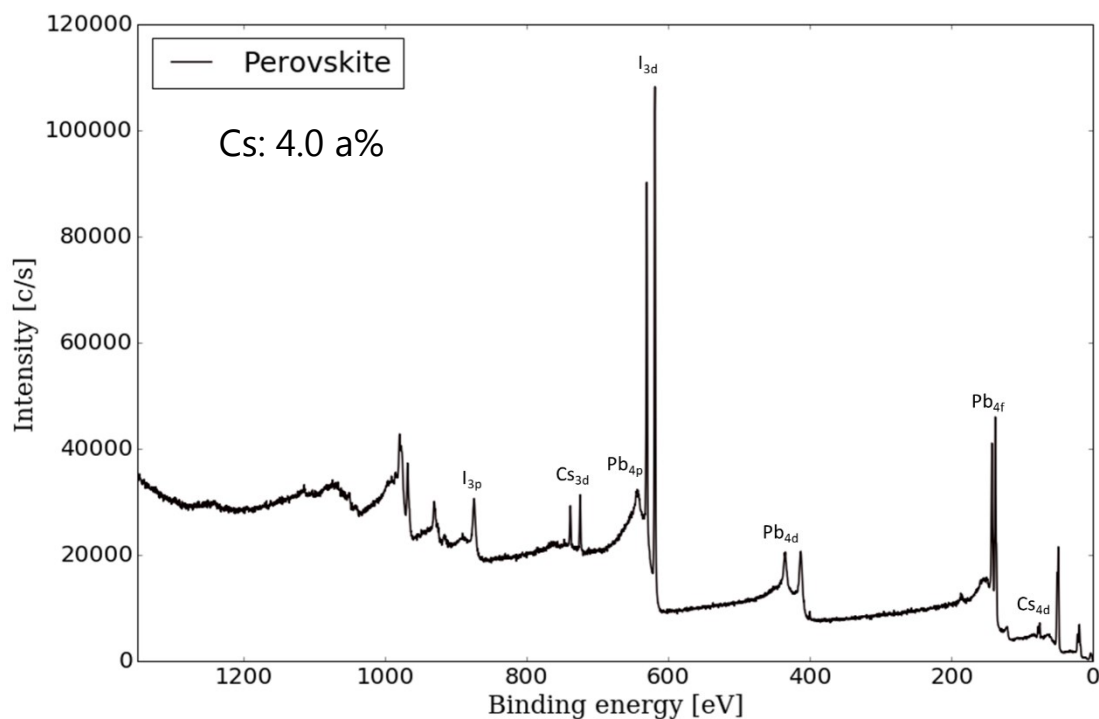


Figure S1: XPS survey scan of perovskite layer deposited by CVD.

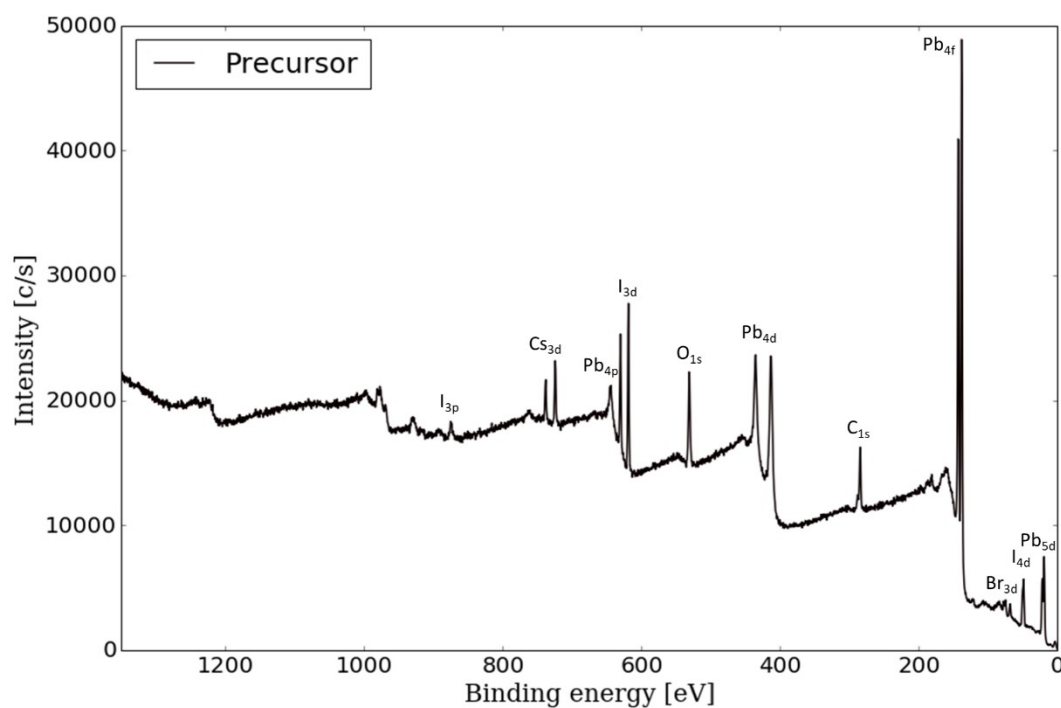


Figure S2: XPS survey scan of CsBrPbI₂ precursor layer deposited by PVD.

2 XPS analysis

3

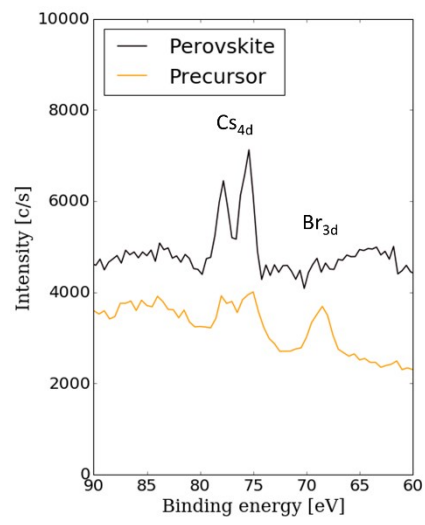


Figure S3: Zoom of XPS spectra. The precursor measurement shows both signals stemming from caesium and bromine while the latter is missing in the case of the perovskite.

4

5

6 Calculation of the conversion fraction

7 Following the approach from Ummadisingu et al.¹, the conversion fraction $\Gamma(t)$ was defined as:

$$\Gamma(t) = \frac{A(t)}{A_{fc}} * 100\%$$

8 where $A(t)$ and is the absorbance after reaction time t and A_{fc} is the
9 absorbance of the perovskite layer after full conversion of the precursor layer. This definition assumes
10 a layered growth of the perovskite layer, where the thickness of the perovskite layer is linear
11 proportional to the absorbance, according to the following derivation.

12 The absorbance is defined as:

$$A = -\log_{10}(T) = \frac{\tau}{\ln(10)}$$

14 where T is the transmittance and τ is the optical depth of the perovskite layer.

15 The optical depth can be calculated the law of Lambert-Beer, which reads as²:

$$I(d) = I_0 * e^{-\tau} = I_0 * e^{-\alpha_{\lambda} * d}$$

16

17

18 where $I(d)$ is the intensity of a (monochromatic) beam with wavelength λ with initial intensity I_0 after
19 passing a material with thickness d and extinction coefficient α (for the specific probing wavelength).

20 The optical depth can then be calculated from:

$$\tau = \alpha_{\lambda} * d = -\ln\left(\frac{I(d)}{I_0}\right) \Big|_{\lambda}$$

21

22 To account for the relatively high reflectance of the plain perovskite layers we corrected the intensity
23 according to the model shown in **Figure S4**.

24 The optical model used for the derivation of the formula assumes reflection at the initial air interface
25 only, and notably neglects reflections at the back interfaces. In our case, the strongest contrast of
26 refractive index (hence the strongest reflection) is indeed at the first air-perovskite interface. Moreover,
27 in the wavelength range of interest (about 600-750 nm), the light reflected at the back interfaces is
28 strongly absorbed (twice) in the perovskite layer and only weakly affects the reflectance spectrum. A
29 wavelength-dependent error remains, caused by the light reflected at the back interfaces not
30 contributing to the transmittance.

31

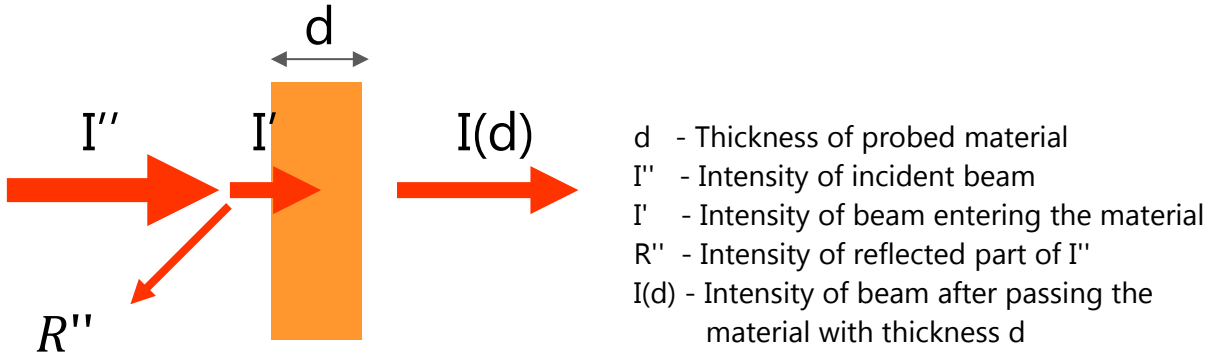


Figure S4: Optical model for the determination of the thickness, respectively the optical depth of the perovskite layer.

32 In short the model assumes that:

33

34

$$I(d) = I'' * \%T/100$$

35 and:

$$I' = I'' - R'' = I'' * (100 - \%R)/100$$

36

37 where %R and %T are the measured reflectance and transmittance in percent, respectively

38 From the model and the Lambert-Beer relationship it follows that:

39

40

$$\tau = \alpha_{\lambda} * d = -\ln\left(\frac{I(d)}{I'}\right)_{\lambda} = -\ln\left(\frac{\%T}{100 - \%R}\right)_{\lambda}$$

41

42 The conversion fraction was in the end calculated by:

$$\Gamma(t) = \frac{\ln\left(\frac{\%T(t)}{100 - \%R(t)}\right)}{\ln\left(\frac{\%T_{fc}}{100 - \%R_{fc}}\right)} * 100\%$$

43

44

45 where %T(t) and %R(t) are the measured transmittance and reflectance of the layer after a conversion

46 time t, %T_{fc} and %R_{fc} are the transmittance and reflectance of a fully converted reference layer.

47

48 Our fully converted reference layer is the sample '08 min 160-210°C' as this sample does not show any

49 residuals of precursor phase in the XRD scan and the samples exhibits the highest absorbance.

50

51 To ensure the robustness of the chosen evaluation method we conducted the estimation calculation in
52 the wavelength range from 600 nm to 750 nm. The data points and the error bars shown in **Figure 2**
53 are the means and double the calculated standard deviations, respectively. As the sample '08 min 160-
54 210°C' was defined as the reference for 100% conversion fraction, it has a standard deviation of zero
55 (i.e., the error bar width is also zero). The complete set of underlying measurements and calculated
56 curves is presented in **Figure S5**. From the results we obtain, we are confident that this method is well
57 suited for the calculation of the conversion fraction. Still we would like to mention that the maximum
58 achievable conversion fraction of a specific sample is defined by the initial thickness of its precursor
59 layer. I.e., that a specific sample will not reach above e.g. 95% conversion fraction if its precursor layer
60 thickness was only at 95% of the thickness of the precursor layer of the reference (i.e., fully converted)
61 sample.

62 **Figure S6** shows a comparison of one of our experimental curves with literature values for MAPbI₃ for
63 different thicknesses. The curves of the literature references were calculated using ellipsometry data
64 from work of Eerden et al.³ and a transfer matrix model of a single layer of perovskite. The result show
65 that the chosen approach is well suited for the evaluation of the relative thickness of the perovskite
66 layer.

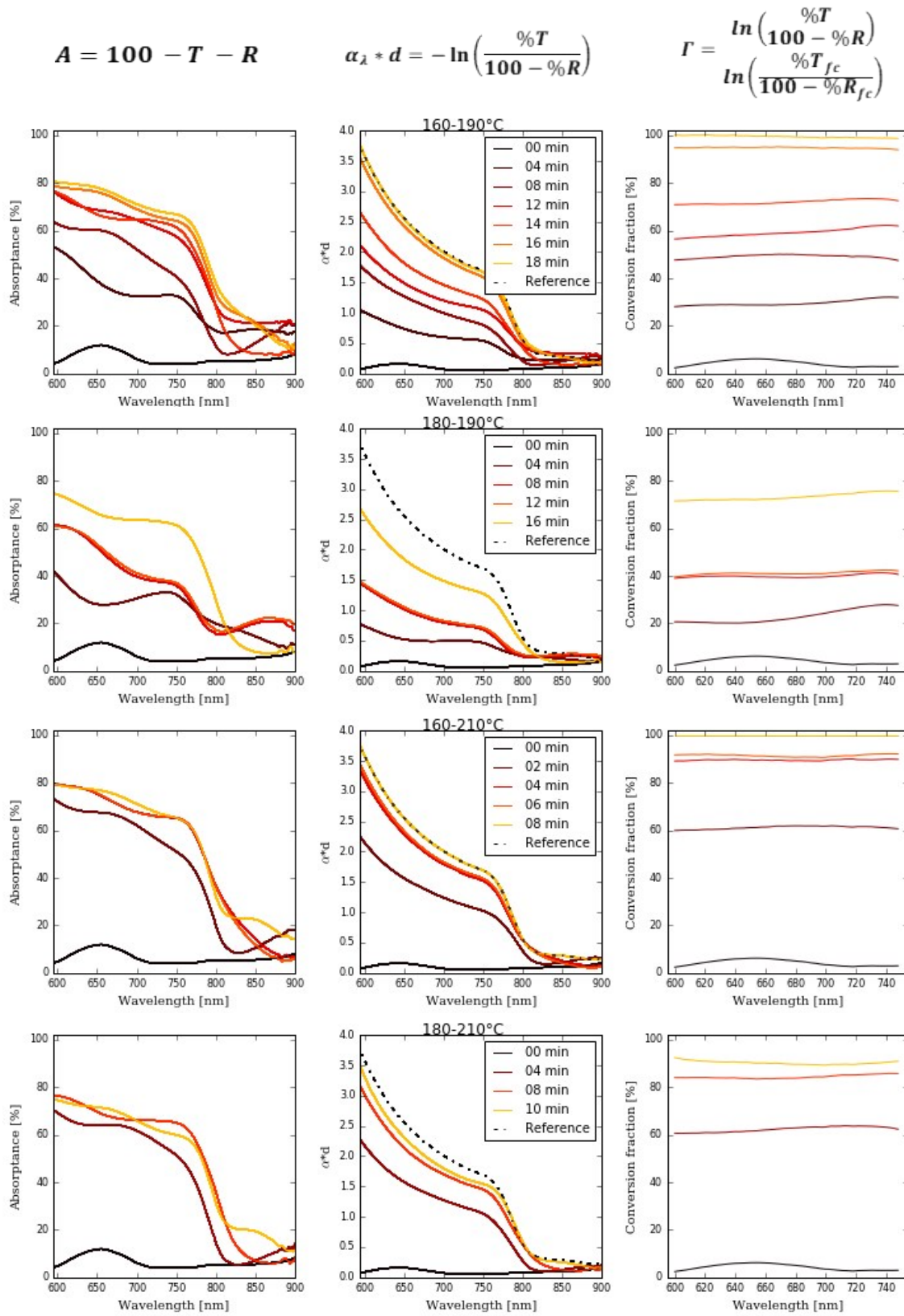


Figure S5: Absorbance, $\alpha \cdot d$ (i.e., optical depth) and the conversion fraction of the sample fabricated at different conditions and different times. The used formulas are given on top of each corresponding column.

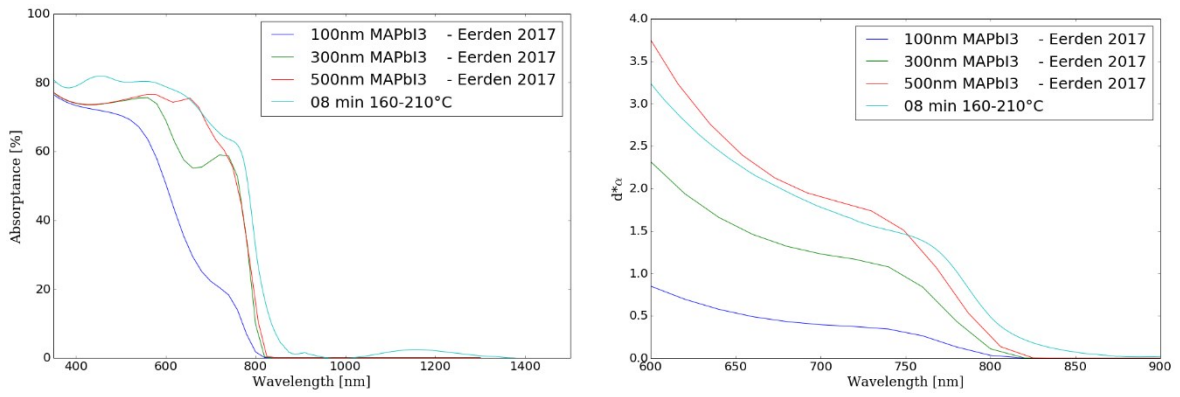


Figure S6: Absorbance (left) and optical depth $\alpha \cdot d$ (right) versus wavelength for fully converted layer from experimental sample ('08 min 160-210°C') and literature data ('Eerden 2017').

68

69

70

71 XRD results

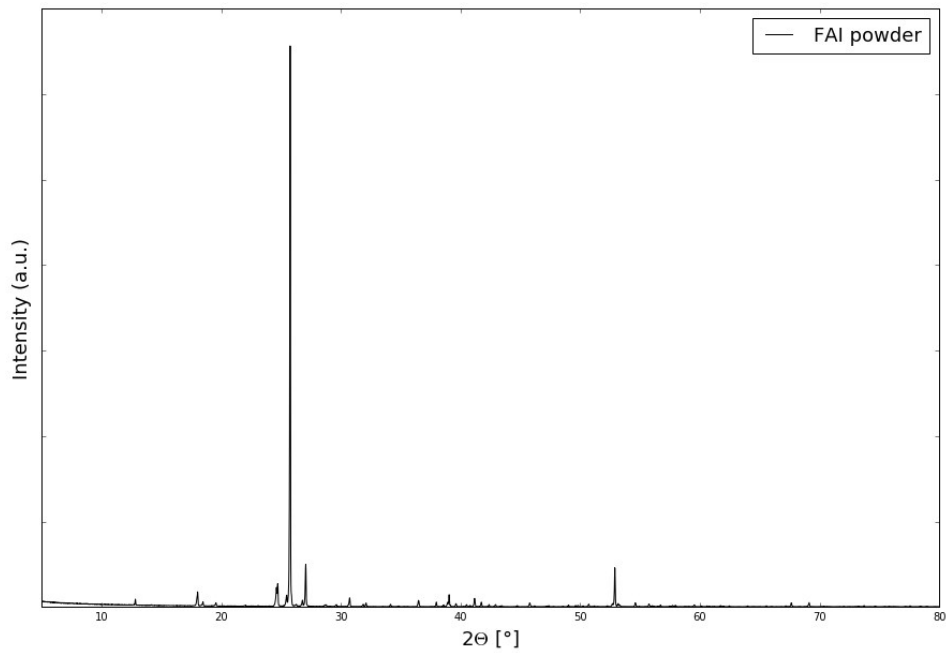


Figure S7: XRD pattern of pure FAI powder used in CVD process

72

73

74

75

76

77 **Grain size analysis**

78 **Figure S8** shows the distribution of grain sizes for different CVD conditions.

79

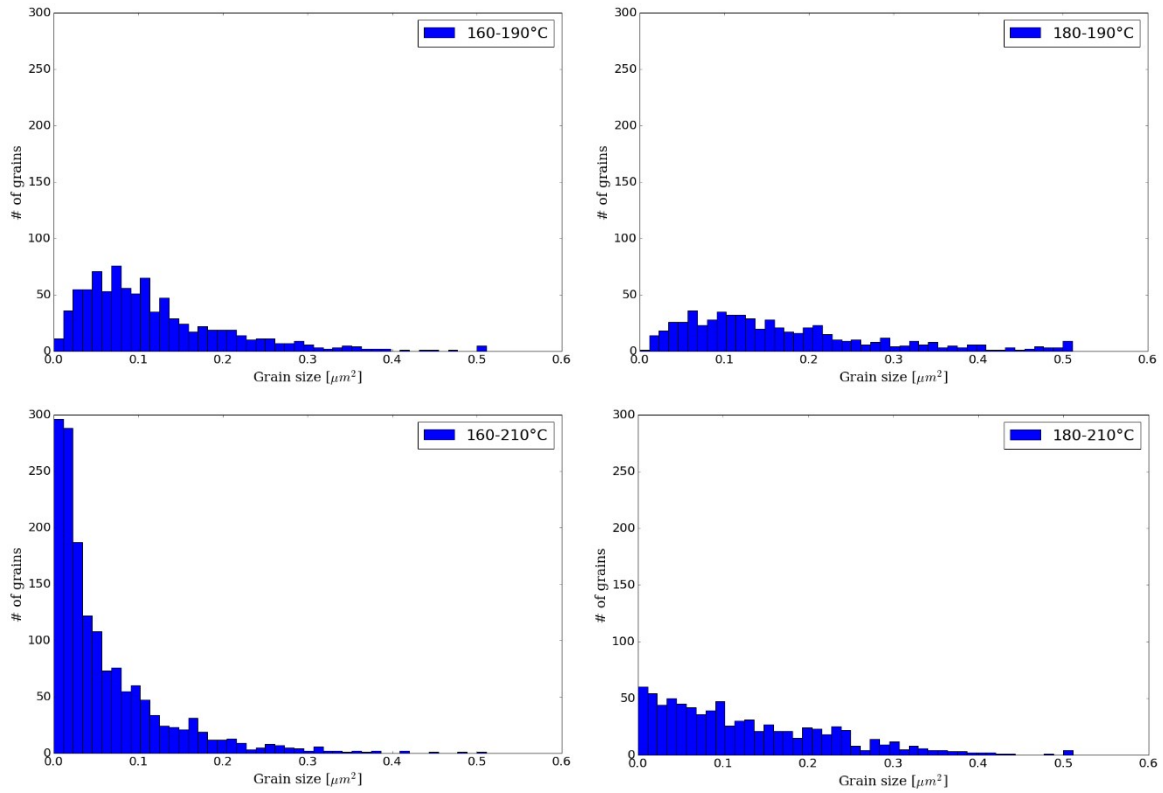


Figure S8: Size distribution of perovskite grains grown under different conditions.

80

81

82

83

84 **SEM micrographs**

85 **Figures S9-11** show the SEM micrographs of layers for different conditions and conversion times.

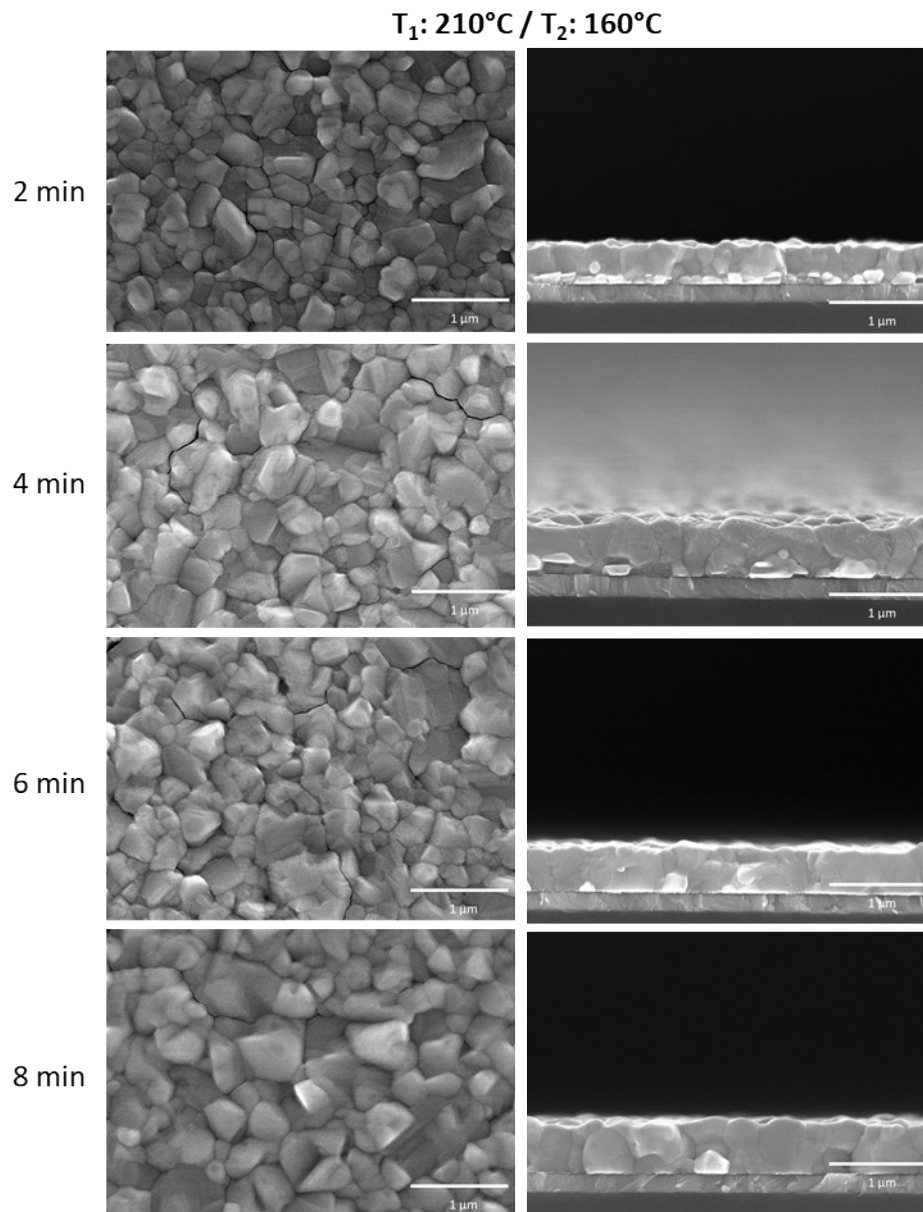


Figure S9: SEM top-view and crosssection of layers processed at conditions 160-210 after different conversion times

86

87

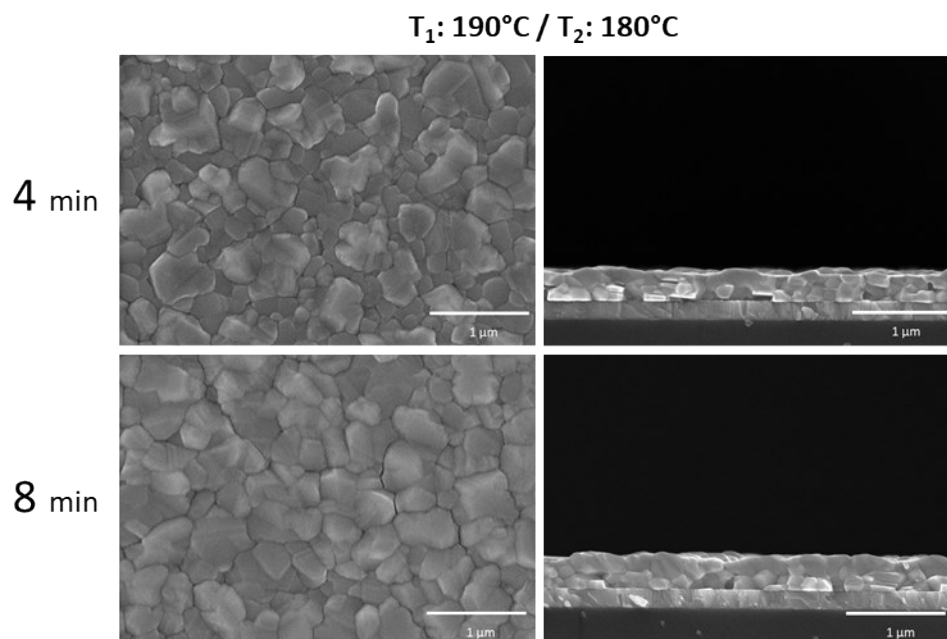


Figure S10: SEM top-view and crosssection of layers converted under condition 180-190 after different conversion times.

88

89

90

91

92

93

94

95

96

97

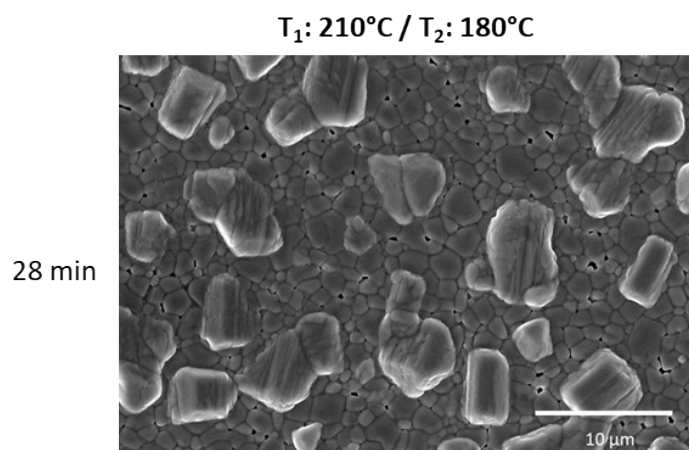


Figure S11: SEM topview of layer converted under condition 180-210 for 28 minutes. Large grains (presumably the overconverted phase) formed on top of a porous bottom layer.

100

101

102

103 **CVD conversion of 5x5 cm substrate**

104 **Figure S12** shows the XRD scans and UV-Vis spectra of different areas of a perovskite layer deposited
 105 by CVD on a 5x5 cm substrate.

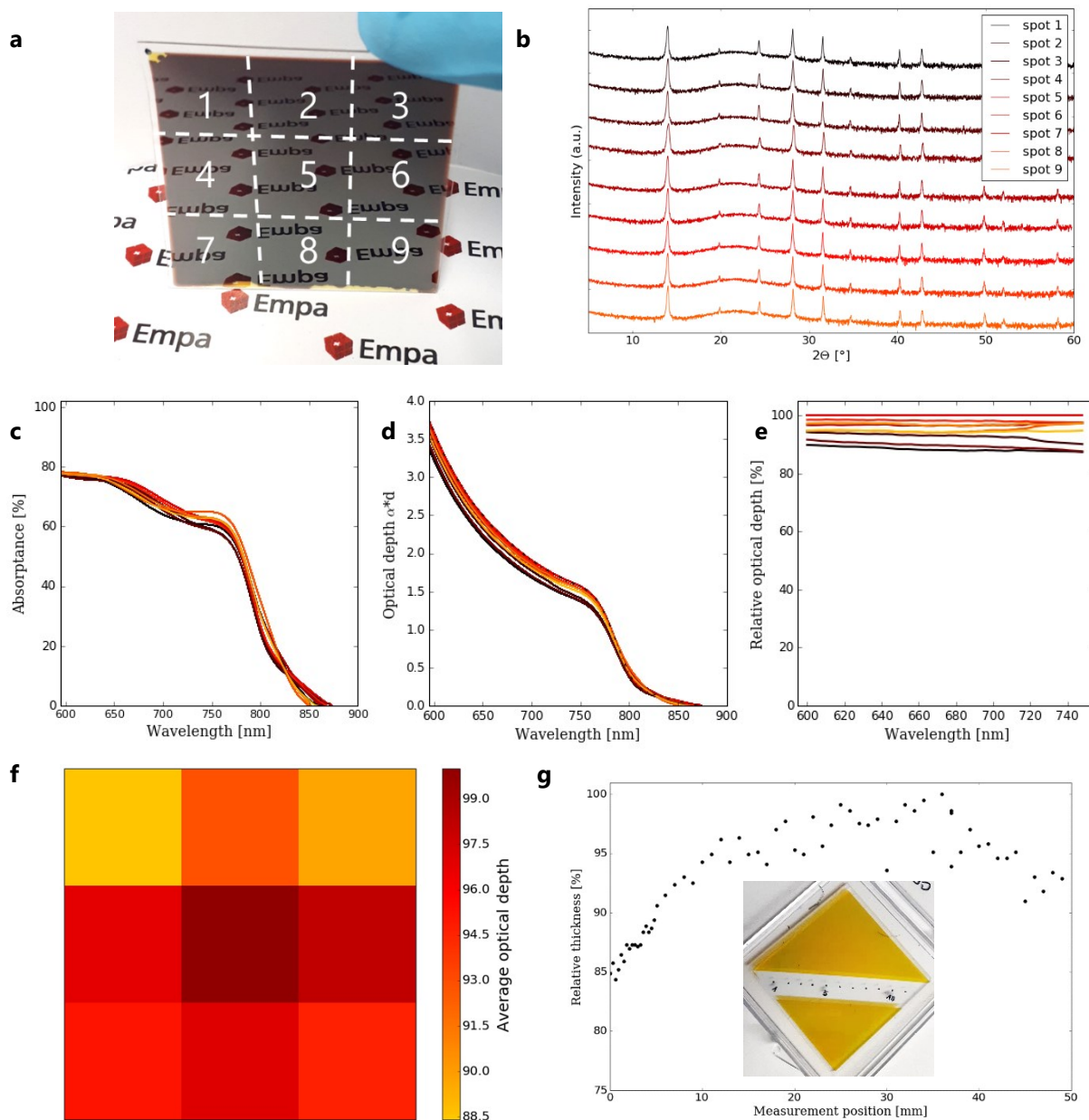


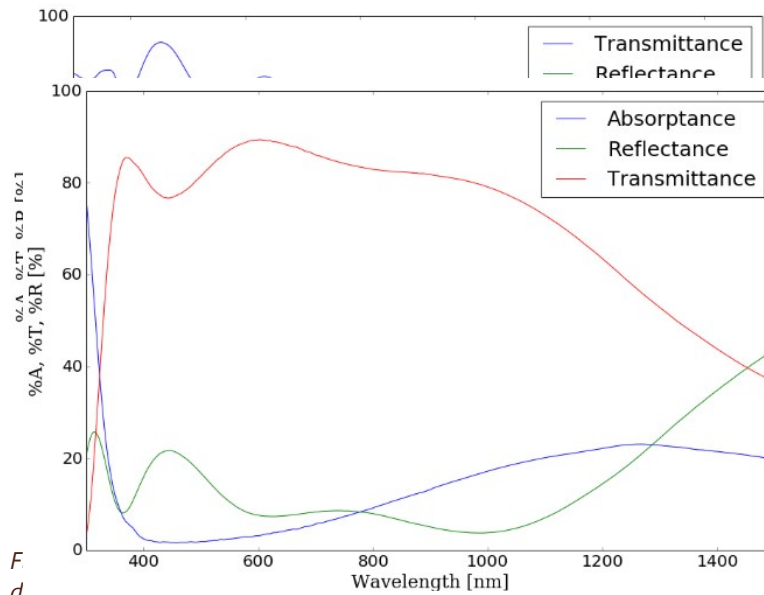
Figure S12: Uniform CVD conversion of a 5x5 cm precursor layer. a) Photograph of the perovskite layer after conversion with the investigated areas indicated. b) XRD scans of each region showing a single perovskite phase all over the substrate. c) UV-Vis response of the individual areas. d) Optical depth of the individual areas. e) Relative optical depth of the individual areas, taking area No. 5 as the 100% reference. f) Average relative optical depth of the individual areas revealing a thinner perovskite layer in the edge/corner areas. g) Relative thickness of the PVD deposited CsBrPbI_2 precursor layer measured along the diagonal of a 5x5 cm substrate. Towards the edges/corners, the precursor layer shows a ~10% lower thickness than in the middle region.

106
 107
 108

109 **Solar cell characterization**

110 **Figure S13** and **Figure S14** show the UV-Vis response of the device stack of the semi-transparent
111 solar cells and the ITO substrate used for the device fabrication.

112



d Figure S14: UV-Vis response of bare ITO substrate. The free carrier absorption strongly reduces the transmittance in the near infrared region.

113
114
115
116
117
118
119
120

121 **Figure S15** shows the statistics of the J-V parameters collected from 9 individual devices shown in the
122 manuscript.
123

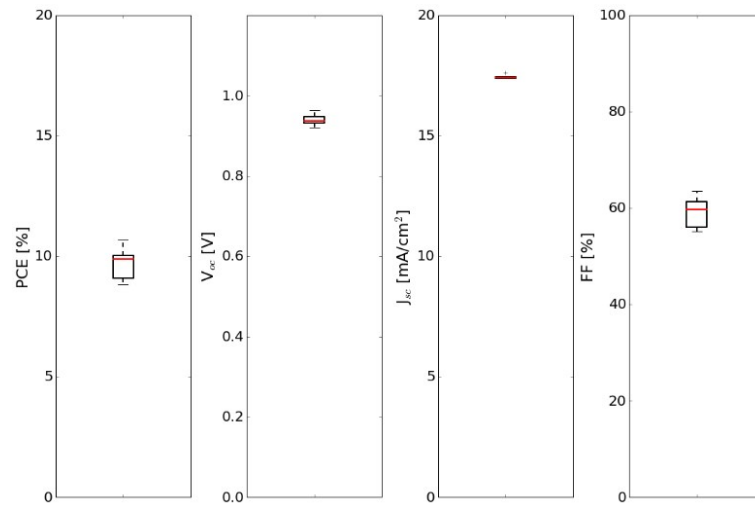


Figure S15: J-V statistics from 9 cells fabricated with PVD-CVD perovskite.

124
125
126
127

128 **References**

- 129 1 A. Ummadisingu and M. Grätzel, *Science Advances*, 2018, **4**, e1701402.
- 130 2 M. Brinkmann, J. Hayden, M. Letz, S. Reichel, C. Click, W. Mannstadt, B. Schreder, S. Wolff, S. Ritter, M.
131 Davis, T. Bauer, H. Ren, Y.-H. Fan, S.-T. Wu, K. Bonrad, E. Krätzig, K. Buse and R. Paquin, in *Springer*
132 *Handbook of Lasers and Optics*, ed. F. Träger, Springer, New York, NY, 2007, pp. 249–372.
- 133 3 M. van Eerden, M. Jaysankar, A. Hadipour, T. Merckx, J. J. Schermer, T. Aernouts, J. Poortmans and U.
134 W. Paetzold, *Advanced Optical Materials*, 2017, **5**, 1700151.
- 135
- 136